



Published in final edited form as:

*Biochem J.* 2009 January 1; 417(1): 195–203. doi:10.1042/BJ20081073.

## Atp6v1c1 is an essential component of the osteoclast proton pump and in F-actin ring formation in osteoclasts

Shengmei Feng<sup>\*,†</sup>, Lianfu Deng<sup>‡</sup>, Wei Chen<sup>†,§</sup>, Jianzhong Shao<sup>\*</sup>, Guoliang Xu<sup>||</sup>, and Yi-Ping Li<sup>\*,†,‡,§,||</sup>

<sup>\*</sup> Life Science College, Zhejiang University, 388 Yuhang Road, Hongzhou 310058, People's Republic of China

<sup>†</sup> Department of Cytokine Biology, The Forsyth Institute, 140 The Fenway, Boston, Massachusetts 02115, USA

<sup>‡</sup> Shanghai Institute of Traumatology and Orthopaedics, 197 Ruijin er Road, Shanghai 200025, People's Republic of China

<sup>§</sup> Department of Developmental Biology, Harvard School of Dental Medicine, 188 Longwood Avenue, Boston, Massachusetts 02115, USA

<sup>||</sup> Institute of Biochemistry and Cell Biology, Shanghai Institutes for Biological Sciences, Chinese Academy of Sciences, 320 Yueyang Road, Shanghai 200031, People's Republic of China

### Synopsis

Bone resorption relies on the extracellular acidification function of vacuolar ATPase (V-ATPase) proton pump(s) present in the plasma membrane of osteoclasts. The exact configuration of the osteoclast-specific ruffled border V-ATPases remains largely unknown. In this study, we found that the V-ATPase subunit Atp6v1c1 (C1) is highly expressed in osteoclasts while subunits Atp6v1c2a (C2a) and Atp6v1c2b (C2b) are not. The expression level of C1 is highly induced by RANKL during osteoclast differentiation; C1 interacts with Atp6v0a3 (a3) and is mainly localized on the ruffled border of activated osteoclasts. Our data show for the first time that C1 silencing by lentivirus-mediated RNA interference severely impaired osteoclast acidification activity and bone resorption, while cell differentiation did not appear to be affected, which is similar to a3 silencing. The F-actin ring formation was severely defected in C1-depleted osteoclasts but not in a3-depleted and a3<sup>-/-</sup> osteoclasts. C1 co-localized with microtubules in the plasma membrane and its vicinity in mature osteoclasts. In addition, C1 co-localized with F-actin in the cytoplasm; however, the co-localization chiefly shifted to the cell periphery of mature osteoclasts. Our study demonstrated that Atp6v1c1 is an essential component of the osteoclast proton pump at the osteoclast ruffled border and that it may regulate F-actin ring formation in osteoclast activation.

### Keywords

Atp6v1c1 (C1); osteoclasts; F-actin ring; acidification; bone resorption; V-ATPase

¶ Corresponding Author: Dr. Yi-Ping Li, Department of Cytokine Biology, The Forsyth Institute, 140 The Fenway, Boston, MA 02115, Tel: 617-892-8260, Fax: 617-262 4021, E-mail: ypli@forsyth.org.

## Introduction

Vacuolar-type proton-translocating ATPases (V-ATPases) are composed of an ATP-hydrolytic domain ( $V_1$ ) and a proton-translocation domain ( $V_0$ ), as well as the accessory subunits ac45 and M8-9 [1]. The  $V_1$  domain is located in the cytoplasm and contains eight different subunits (A–H): the catalytic nucleotide-binding subunit A, the non-catalytic nucleotide-binding subunit B (stoichiometry of A3:B3), and the stalk subunits C–H (proposed stoichiometry of C1:D1:E1:F1:G2:H1) [2–4]. The  $V_0$  domain, an integral membrane bound domain, connects to the  $V_1$  domain by the central and peripheral stalks. In mammals, the  $V_0$  domain consists of a, c, c', c'', e and d subunits. V-ATPases are involved in a wide variety of physiological processes, including endocytosis, intracellular membrane trafficking, macromolecular processing and degradation, and ligand-coupled transport, but they are primarily responsible for the acidification of intracellular compartments in all eukaryotic cells [3;5]. For their diverse functions, V-ATPases utilize specific subunit isoform(s) in specific cells and cell organelles. For instance, a4, B1, C2b, d2, and G3 are highly expressed in the kidney and epididymis [6–10]; a1 and G2 are highly expressed in the brain [11]; and a3, B2, and d2 are highly expressed in osteoclasts [9;12;13]. Osteoclasts are the principal cells responsible for bone resorption. Their ruffled membrane V-ATPases tightly coupling to a passive chloride channel are required for acidification of the resorption lacunae and bone matrix demineralization [14]. Therefore, we reason that osteoclast V-ATPases present in the ruffled border are comprised of unique subunits such as a3, B2, and other unknown subunits, which are different from other V-ATPases [12;15]. In this study, we defined another subunit of the osteoclast proton pump.

As we know, in mouse V-ATPase there are three isoforms of subunit C: Atp6v1c1 (C1), Atp6v1c2a (C2a), and Atp6v1c2b (C2b). C1 is expressed ubiquitously, but C2a is a lung-specific isoform containing a 46-amino acid insertion and C2b is a kidney-specific isoform without the insert [10;16]. Despite these insights, the possible role of C1 as an essential component of the osteoclast proton pump; C1's function in an osteoclast proton pump; its localization in activated osteoclasts; and its function in the differentiation, maturation, acidification, and bone resorption of mature osteoclasts, remain unclear.

In multinucleated osteoclasts, bone resorption is active in the ruffled border surrounded by a tight sealing zone, which contains highly dynamic actin-containing adhesion structures known as podosomes. These podosomes are composed of a small filamentous actin (F-actin) column surrounded by proteins such as vinculin and paxillin. Protons and enzyme secretions are restricted to the resorption lacuna, limited by the sealing zone. However, in mature osteoclasts seeded on glass or plastic, podosomes form a belt on the cell periphery [17–19]. Previous reports showed that the formation of actin sealing rings was severely impaired in osteoclasts deficient in Atp6v0d2 [20], while formation was uncertain in Atp6v0a3 deficient osteoclasts [21;22]. These results prompted us to wonder whether V-ATPase subunits are also involved in F-actin ring formation during osteoclast activation. Recently, Vitavska et al. reported that in vitro subunit C can directly bind and stabilize F-actin, increase the initial rate of actin polymerization in a concentration-dependent manner, and cross-link actin filaments to bundles of varying thickness [23;24]. According to these findings we speculate that subunit C1 may be involved in F-actin ring formation during osteoclast activation.

Here we show that subunit C1 is highly expressed in mouse osteoclasts and that its expression can be induced by receptor activator of NF- $\kappa$ B ligand (RANKL) and macrophage-colony stimulating factor (M-CSF) during osteoclast differentiation. The acidification activity and the bone resorption function of C1-depleted cells were severely impaired, but osteoclast differentiation and maturation were normal. Furthermore, immunohistochemistry showed that C1 was expressed mainly in the ruffled membrane. The co-IP assay showed that C1 interacts

with subunit  $\alpha 3$  and that C1 co-localized with microtubules in the plasma membrane and its vicinity in mature osteoclasts. We also found that F-actin ring formation was severely defected in C1-depleted osteoclasts and that C1 co-localized with F-actin both in the cell periphery and in the cytoplasm of mature osteoclasts.

## Experimental

### Cells and cell culture

The mature osteoclasts in primary culture were generated from bone marrow-derived monocytes (BMMs) as described [25]. Briefly, BMMs were isolated from tibiae and femurs from six-week-old C57BL6 mice.  $1-2 \times 10^5$  BMMs were seeded into a well of a 24-well plate and  $1 \times 10^6$  BMMs were seeded into a well of 6-well plate. The cells were cultured in  $\alpha$ -MEM containing 10% FBS, 10 ng/ml RANKL, and 10 ng/ml M-CSF at 37°C in a humidified atmosphere containing 5% CO<sub>2</sub> for 4 to 6 days. As a control, a monocytic osteoclast progenitor cell line MOCP-5 that was generated in our laboratory [26], was also induced into multinuclear OCLs in  $\alpha$ -MEM containing 10% FBS, 10 ng/ml RANKL, and 10 ng/ml M-CSF for 4 days [26].

### GeneChip analysis

Total RNA was extracted from human osteoclastoma and stromal cells using Trizol reagent (Life Technologies, Inc.), as described by the manufacturer. GeneChip analysis was performed by the Microarray Core Facility at Harvard Medical School. In brief, equivalent amounts of mRNAs from osteoclastoma and stromal cells were reverse transcribed into cDNA, labeled with reporter molecules (Cy3 and Cy5), and tested by simultaneously hybridizing the two cDNAs probes to a DNA microarray. The data were analyzed using an Affymetrix GeneChip scanner and accompanying gene expression software. We compared the signal intensity of *Atp6v1c1* and *Atp6v1c2* in human osteoclast samples. A comparison of *Atp6v1c1* in stromal cells and human osteoclast samples was derived from the resulting intensity ratios.

### Preparation of RNA samples and Reverse Transcription-PCR (RT-PCR) analysis

Total RNA was isolated from cultured cells or mouse tissues with Trizol reagent (Invitrogen) according to the manufacturer's protocol. Mouse cDNA was reverse-transcribed from 0.5  $\mu$ g total RNA with oligo(dT)<sub>15</sub> primer by AMV Reverse Transcriptase (Promega) following the manufacturer's standard method. 10% of the resulting cDNA was used for cloning the 1.15 kb full length coding sequence of *Atp6v1c1* (accession no. NM\_025494.2) with the following primers: *c1-cds-F* 5'-CGCGGATCCAACATGACTGAGTTCTGGCTC-3' and *c1-cds-R* 5'-CCGCTCGAGTTACTTGAATCCAGCAAGTTG-3'. Each RT-PCR assay was performed with an aliquot of 2% of the resulting cDNA with gene-specific primers as follows: for *Atp6v1c1* (expected product of 523 bp) sense 5'-AATAATCTTGCCGTCTTCC-3' and antisense 5'-GCGTTTCATACTGCTTAATCC-3', for *Atp6v1c2* (common primers for c2-a and c2-b; expected product of 433 bp) sense 5'-AACTTCAAAGTCTAACCTGTCC-3' and antisense 5'-GACAATATCGCTCAGTGTCC-3', and for  $\beta$ -actin (expected product of 517 bp) sense 5'-CATTGAACATGGCATTGTTACC-3' and antisense 5'-CAGCTCATAGCTTCTCCAGG-3'. All RT-PCR assays were repeated three times. The product fragments were resolved by electrophoresis in 1% agarose gel. Semi-quantitative analysis was performed with Labworks 4.6 software.

### Preparation of antibodies

Rabbit antibodies against synthetic peptides: *Atp6v1c1* <sup>12</sup>EKTCQQTWEKLHAA TTK<sup>28</sup> [16],  $\alpha 3$  <sup>816</sup>CFYSGTGYKLSPTFTVDS<sup>834</sup>, and *Atp6v1a* <sup>603</sup>CQLLEDMQN AFRSLED<sup>617</sup> [8] were generated by coupling peptides to KLH and immunizing rabbits. The

monoclonal antibody against GAPDH (14C10), anti-rabbit IgG, and anti-mouse IgG (HRP-linked antibody) were purchased from Cell Signaling. Anti-FLAG M2, anti-GFP, and anti-actin monoclonal antibodies were purchased from Sigma. Goat-anti-rabbit-FITC and goat-anti-mouse-TR were purchased from Santa Cruz Biotechnology.

### Selection of siRNA and Western blotting

Small interference RNA (siRNA) was designed from Dharmacon siDESIGN center (<http://www.dharmacon.com>) specifically targeting mRNA of *Atp6v1c1* with the sequences of c1s1: 5'-TTCGTGACTTCCAGTATAA-3', c1s2: 5'-TTGCGTGGATTCATATAAA', c1s3: 5'-GAGTTGACTTGGTTACTTA-3', and specifically targeting mRNA of *Atp6v0a3* with the sequence of si-a3: 5'-GTATCCTCATTCACTTCAT-3'. The negative control siRNA targeting LacZ (si-LacZ) is 5'-CTCGGCGTTTCATCTGTGG-3'. The short hairpin RNA (shRNA) oligos were annealed and ligated into the *Bgl*II/*Hind*III-site of pSUPER. The shRNA was then validated by determining the depletion effect on the expression of co-transfected Flag-C1 in human embryonic kidney 293T (HEK293T). Briefly, resulting plasmid constructs were co-transfected into HEK293T cells with the plasmid of Flag-C1 using lipofectamine reagent (Invitrogen) in duplicate on three independent occasions. Cells were harvested into standard lysis buffer (50 mM Tris-HCl, pH 6.8, 100 mM dithiothreitol, 2% SDS, 0.001% bromophenol blue, 10% glycerol). SDS/PAGE and Western blotting analysis were carried out according to a standard protocol with the anti-Flag monoclonal antibody (1:10000), anti- $\beta$ -actin monoclonal antibody (1:3000), and anti-GFP monoclonal antibody (1:10000).

### Preparation of lentivirus and infection

The effective H1 promoter shRNA expression cassettes, c1s3, si-a3, and si-LacZ, were subcloned into the lentivirus transfer vector pLB (Addgene) [27]. This was co-transfected with the packaging plasmids, pCMV-Dr8.2 and pCMV-VSV-G (Addgene) [28], into HEK293T cells using a calcium phosphate co-precipitation method. The medium was replaced with fresh DMEM after co-transfection for 8 hours. The lentiviral supernatant was harvested after 48-72 hours and titers were determined by infecting HEK293T cells with serial dilutions of concentrated lentivirus in the presence of 4  $\mu$ g/ml polybrene (Sigma). For depletion of C1 in osteoclasts, BMMs were induced with M-CSF/RANKL for 48 hours and then transduced with lentiviral supernatant for 8 hours. The medium was replaced with fresh  $\alpha$ -MEM containing 10% FBS, 10 ng/ml RANKL, and 10 ng/ml M-CSF for primary culture. Osteoclasts were harvested for Western blot analysis or for functional experiments 3.5 days after infection.

### TRAP staining

Tartrate-resistant acid phosphatase (TRAP) staining was used as a marker for mature osteoclasts. Cells were fixed and stained for TRAP activity using a Leukocyte acid phosphatase kit (Sigma). Pre-osteoclasts and mature multinucleated osteoclasts (more than three nuclei) appeared dark red and were counted by light microscopy, the experiment was performed in duplicate on five independent occasions. Ten fields were counted for each group. All data are expressed as mean  $\pm$  s.d. (n=10).

### Pit formation assay

Bone resorption activity was assessed by pit formation assay performed according to the method of Chen et al. [26] with slight modification. BMMs were cultured on dentin slices in 96-well plates and infected with lentiviral siRNA after 48 hour induction by RANKL and M-CSF. After 6 days the slices were placed for 10 minutes in 1 M NH<sub>4</sub>OH and were sonicated to remove the cells. The cell-free slices were stained in 1% toluidine blue in 1% sodium borate for 1 minute [29]. The experiment was repeated three times. The resorption pits appeared dark blue and were viewed by light microscopy. The percentage of pit area to a "random field of

view” was counted. Three fields were counted for each group. All data are expressed as mean  $\pm$  s.e.m. (n=3).

### Acridine orange staining

Acid production was determined using acridine orange as described previously [13]. Osteoclasts were incubated in  $\alpha$ -MEM containing 5  $\mu$ g/ml of acridine orange (Sigma) for 15 minutes at 37°C, washed, and chased for 10 minutes in fresh media without acridine orange. The cells were observed under a fluorescence microscope with a 490 nm excitation filter and a 525 nm arrest filter. The experiment was performed in duplicate on four independent occasions in a 24-well plate.

### Cell staining for F-actin rings

Cells were fixed with 3.7% formaldehyde and permeabilized with 0.2% Triton X-100. The cells were then blocked with 1% goat serum and 3% BSA and incubated with 2 U/ml rhodamine phalloidin (Molecular Probes) at room temperature for 20 minutes. Nuclei were visualized with 1  $\mu$ g/ml DAPI (Sigma). The experiment was performed in duplicate on four independent occasions in a 24-well plate.

### Cell immunofluorescence

BMMs were grown on 6 cm dishes and induced by RANKL and M-CSF for 5 days. Then they were fixed with 2% formaldehyde in phosphate-buffered saline (PBS) for 20 minutes, washed with PBS 3 times, incubated in 0.2% Triton X-100 for 15 minutes, and blocked for one hour with 10% normal goat serum in PBS. Additionally, cells were incubated in the primary antibody ( $\alpha$ -Atp6v1c1, 1:50;  $\alpha$ -microtubules, 1:2), diluted in 1% normal serum in PBS overnight at 4°C, washed three times with PBS for 5 minutes, and incubated with either secondary antibody goat-anti-rabbit-FITC (1:50) and rhodamine phalloidin, (1:100) or with goat-anti-mouse-TR (1:50) for 1 hour. Cells were then washed with PBS and mounted with anti-fade mounting medium (gift from Dr. Shi-liang Ma). Observations were performed by epifluorescence in a Zeiss axioplan microscope. The experiments were set in triplicate on three independent occasions.

### Immunohistochemistry

Immunohistochemistry was performed as described previously [13]. Briefly, mice (C57Bl/6J male; age 6 weeks) were anesthetized and then perfused with 4% paraformaldehyde in PBS (pH 7.4). Their tibiae and femora were dissected out and immersed in the same solution overnight at 4°C. Then they were sectioned at 6  $\mu$ m thickness and mounted on gelatin-coated slides. Endogenous peroxidase activity was quenched with 0.3% hydrogen peroxide in PBS for 20 minutes. Nonspecific background staining was blocked by incubating sections in 10% goat serum in PBS for 20 minutes. Primary antibody ( $\alpha$ -Atp6v1c1, 1:600) was applied overnight at 4°C. The horseradish peroxidase avidin-biotin complex system (Rabbit Elite ABC Kit; Vector Laboratories) was used to visualize bound antibody, and sections were counterstained with 0.1% Fast Green (VWR). The experiments were set in triplicate on three independent occasions.

### Co-immunoprecipitation

BMMs were stimulated with RANKL and M-CSF for 5 days and then washed with cold PBS and lysed in a buffer containing 20 mM Tris (pH 7.4), 150 mM NaCl, 1% NP-40, and protease inhibitors (Sigma) [30]. Following a centrifugation at low speed (20 minutes at 14,000 g, 4°C) to remove insoluble material, cell lysates were incubated at 4°C for 2 hours with  $\alpha$ -Atp6v1c1 (1:1000) and then incubated with protein A/G Sepharose beads (Santa Cruz Biotechnology)



overnight. The precipitates were separated by 8% SDS-PAGE, followed by immunoblotting as described previously [30]. The experiment was repeated five times.

## Results

### *Atp6v1c1* is highly expressed in mouse osteoclasts

We have characterized *Atp6v0a3* as an osteoclast-specific isoform of subunit a that is essential in osteoclast-mediated extracellular acidification in bone resorption [13], suggesting that additional specific subunit isoforms may exist as components of the osteoclast ruffled border V-ATPase proton pump. In this study, we determined whether there are other specific subunit isoforms in the osteoclast ruffled border proton pump using microarray to analyze osteoclast mRNA gene expression profiles as described [25;31]. We found that the level of *Atp6v1c1* (*C1*) expression was nearly 139-fold higher than *Atp6v1c2* (*C2*) expression in human osteoclasts (Figure 1A), and *C1* expression in human osteoclasts was nearly 42-fold higher than that in stromal cells (Figure 1B).

Microarray data showed that *C2* is weakly expressed in osteoclasts (Figure 1A). To define whether the two isoforms of *C2* are expressed in osteoclasts, we designed primers shared by both *C2a* and *C2b* to perform semi-quantitative RT-PCR assays on eight mouse tissues and six related cell lines (Figure 1C). *C2* was detected in brain, lung, kidney, and embryonic stem cells (ES), but not in BMMs, MOCP-5 (an osteoclast precursor cell line) [26], osteoclasts (OC), or osteoclast-like cells (OCLs derived from MOCP-5; Figure 1C middle). Microarray data showed that *C1* was highly expressed in osteoclasts (Figure 1A,B), rather than in stromal cells (Figure 1B). To verify the high expression of *C1* in osteoclasts, we performed gene-specific semi-quantitative RT-PCR. *C1* expression was not detected in osteoblasts, BMMs, or MOCP-5, but it showed an induced expression in osteoclasts and OCLs. *C1* was expressed in osteoclasts at a level as strong as that of brain, kidney, and testis (Figure 1C top). We further quantified the expression of *C1* normalized to  $\beta$ -actin level, and found that *C1* expression was highly induced by RANKL and M-CSF (nearly 16-fold; Figure 1D). To test whether *C1* protein expression can also be induced by RANKL and M-CSF, BMMs were treated with RANKL and M-CSF for the indicated time (Figure 1E). We used Western blotting to detect *C1* expression (Figure 1E). *C1* protein was detected on day 2, continued to increase through day 4, and stayed at high levels until 7 days after stimulation with RANKL and M-CSF (normalized to the  $\beta$ -actin level; Figure 1F). These results indicated that *C1* is much more highly expressed in osteoclasts than *C2*, and that *C1* expression can be induced by RANKL and M-CSF during osteoclast differentiation.

### Effective depletion of *Atp6v1c1* expression by lentiviral siRNA in osteoclasts in primary culture

*Atp6v1c1* is much more highly expressed in mature osteoclasts, so we hypothesize that *C1* plays an important role in osteoclast differentiation and function. To address this point, we used lentiviral constructs encoding siRNAs that target *Atp6v1c1* to infect osteoclasts in primary culture and deplete *C1* expression. We first validated the effect of siRNA on cDNA of Flag-*C1* in HEK293T cells. One of the three siRNAs (c1s3) was shown to deplete 98.8% of the expression of Flag-*C1* in HEK293T by Western blotting with anti-Flag antibody (Figure 2A,B) in contrast to siRNA specific targeting to LacZ and vector. However, the other two siRNAs (c1s1 and c1s2) knocked down only about 27% and 34% of *C1* expression, respectively, compared with LacZ-siRNA (Figure 2B). We therefore used siRNA-c1s3 to clone into the lentivirus transfer vector pLB and to package lentivirus in HEK293T for infection in the primary cultured osteoclasts after 48-hour induction by RANKL and M-CSF. Western blotting confirmed that the depletion of *C1* was effective (Figure 2C,D). Lentiviral infection itself did not cause any change in *C1* expression since control osteoclasts infected with LacZ-siRNA

lentivirus (Lenti-LacZ) showed similar protein levels as untreated osteoclasts (Mock; Figure 2C). In a3-siRNA lentivirus (Lenti-a3) treated osteoclasts, a3 expression was knocked down by 86%, but C1 was not knocked down and there was no difference in expression of *Atp6v1a* among the Mock, Lenti-LacZ, Lenti-c1s3, and Lenti-a3 treated osteoclasts (Figure 2C). Taken together, these results indicate an effective and specific depletion of C1 by siRNA in primary cultured osteoclasts.

### Osteoclasts depleted of *Atp6v1c1* show normal cell differentiation and maturation

Lee et al. reported that *d2* deficiency did not affect osteoclast differentiation but did affect pre-osteoclast fusion [20]. Based on this finding, we wondered whether C1 could also be involved in osteoclast differentiation and maturation. To address this question, we performed a TRAP staining assay. First, for lentivirus-mediated *Atp6v1c1* knockdown, optimal viral particle numbers for infection were based on infection efficiency, determined from the percentage of target cells with green fluorescent protein (GFP), which is expressed independently from the RNAi sequence. We used 200  $\mu$ l lentivirus supernatant to infect  $1 \times 10^5$  BMMs after 48-hour induction by RANKL and M-CSF. After another 48-hour period, infected GFP<sup>+</sup> cells were viewed under fluorescence microscopy (Figure 3A). We then assessed the differentiation and maturation of *C1*-depleted osteoclasts by TRAP staining assay 3.5 days after infection (Figure 3B). The number of stained multinuclear TRAP<sup>+</sup> osteoclasts (TRAP<sup>+</sup> multinucleated cells [MNCs] with  $\geq 3$  nuclei) growing on a 24-well plate reached at least 3.8 in a random view in each group with no significant difference among the groups of Mock, Lenti-LacZ, Lenti-c1s3, and Lenti-a3 (Figure 3C). The percentage of TRAP<sup>+</sup> MNCs ( $\geq 3$  nuclei) in all TRAP<sup>+</sup> cells was also not significantly different among these groups (Figure 3D). These observations indicate that normal differentiation and maturation is sustained in osteoclasts lacking C1 by *C1* knockdown. Taken together, the TRAP staining analysis suggests that knockdown of *C1* does not impair differentiation and maturation of osteoclasts.

### Depletion of *Atp6v1c1* blocks osteoclast acidification activity and decreases bone resorption of osteoclasts

We have detected C1, but not C2a or C2b, expressed in osteoclasts. Furthermore, C1 expression was highly induced by RANKL and M-CSF during osteoclast differentiation (Figure 1C, D, E, F), so we postulated that C1 may play a role as an essential component of the osteoclast ruffled border V-ATPase. Therefore, we further tested the effect of depletion of C1 on osteoclast acidification activity and bone resorption ability using lentiviral constructs encoding siRNA targeting *Atp6v1c1* and *Atp6v0a3* (as a knockdown control) to infect osteoclasts in primary culture. After infection, we measured the acidification activity by vital staining of osteoclasts with acridine orange [32]. In the mock and Lenti-LacZ control osteoclasts, strong orange-red fluorescence indicated active production of H<sup>+</sup> and extracellular acidification (Figure 4A). In comparison, the Lenti-c1s3 and Lenti-a3 treated osteoclasts both displayed little orange-red staining. This result indicates a block of acidification activity due to the knockdown of *C1* and also *a3*, similar to previous results [13]. Furthermore, we reasoned that C1 may play a role like a3 in osteoclast bone resorption, the major function of osteoclasts. To examine potential functions of C1 in bone resorption, we then assessed resorption pit formation by *C1*-knockdown osteoclasts on dentin slices. As shown in Figure 4B, we found reduced pit formation of osteoclasts depleted of *Atp6v1c1* on dentin slices, which is similar to reduced pit formation of osteoclasts depleted of *a3* on dentin slices. Furthermore, pit depth of *C1*-depleted osteoclasts and *a3*-depleted osteoclasts are both much shallower than that of normal osteoclasts. We then assessed the percentage of pit area in a view area and found that the percentages in two control groups (mock and Lenti-LacZ) were both about 40%. By contrast, siRNA-treated osteoclasts formed pit areas accounting for only 0.2-0.3% of a view area (Figure 4C). Taken together, these results strongly suggest that C1, like a3, is an essential component of the ruffled border V-ATPase for the function of osteoclasts.

### **Atp6v1c1 localizes in vivo in activated osteoclasts, it co-localizes with microtubules only in the cytoplasm in vitro in mature osteoclasts, and it interacts with a3 in osteoclasts**

We found that C1 depletion severely impaired osteoclast acidification and bone resorption (Figure 4A,B). So, we further defined whether C1 is a component of the osteoclast ruffled border proton pump. To address this question, we tested C1 localization in vivo in activated osteoclasts by performing immunostaining analysis and found that C1 expression in osteoclasts was much higher than in the surrounding tissue, and that the main staining was at the ruffled border (Figure 5A). We further performed co-IP assay and found that C1 interacted with a3, which is another essential subunit of the osteoclast ruffled border V-ATPase, but C1 did not interact with subunit A (Figure 5B). Subunit a3 has been found to co-localize with microtubules in mature osteoclasts but not with F-actin [33], so we tested whether C1 also co-localizes with microtubules. Interestingly, we found that C1 co-localized with microtubules and that the co-localization polarized to the plasma membrane and its vicinity in mature osteoclasts, just as a3 had previously demonstrated. C1 staining, however, was largely in the cell periphery of mature osteoclasts (Figure 5C). Taken together, these results suggest that C1 is a subunit of the osteoclast ruffled border V-ATPase, and that its interaction with the a3 subunit may be involved in linking the V<sub>1</sub> and V<sub>0</sub> domains together.

### **Depletion of Atp6v1c1 blocks osteoclast F-actin ring formation**

In bone, the osteoclast cytoskeleton is reorganized during the transition from a motile to a resorbing cell to form a F-actin ring that contains a tight sealing zone [34]. Atp6v0d2 was reported to be involved in the formation of F-actin rings [20]. Some researchers reported that Atp6v0a3 is also involved in F-actin ring formation, [22] while others reported that a3-deficient osteoclasts have normal F-actin rings [21]. In vitro, subunit C can cross-link actin filaments to bundles of varying thickness [23]. Here, we found that bone resorption was severely impaired in C1-depleted osteoclasts (Figure 4B). Interestingly, C1 largely localized in the cell periphery as a belt in mature osteoclasts (Figure 5C). Therefore, we speculated that the reduced acidification activity of C1-depleted osteoclasts and their probable inability to form normal F-actin sealing rings would contribute to their reduced bone resorption (Figure 4A). To study the effect of C1 knockdown on osteoclast actin sealing ring formation, we performed phalloidin staining for F-actin rings. As shown in Figure 6, typical red-stained organized F-actin belts at the cell periphery were seen in osteoclasts of control groups (mock, lenti-LacZ, Lenti-a3, and a3<sup>-/-</sup> osteoclasts), but disorganized F-actin-containing patches were commonly found in C1-knockdown osteoclasts (white arrow). In each cell with an F-actin ring, there were at least 3 nuclei stained by DAPI. Our result indicated that C1 deficiency severely impaired F-actin ring formation and a3 deficiency did not affect F-actin ring formation.

### **Atp6v1c1 co-localizes with F-actin in osteoclasts**

According to our interesting finding that C1-depleted osteoclasts showed defective F-actin rings (Figure 6) and C1 staining was largely in the cell periphery as a belt (Figure 5C), we further wondered whether C1 and F-actin co-localize in osteoclasts. To address this question, we performed immunofluorescence as shown in Figure 7A-7L. Besides their co-localization in the cytoplasm (Figure 7D, G, H; single red arrow), C1 localization moved to the cell periphery along with the F-actin ring (double red arrow) in mature activated multinuclear osteoclasts. In contrast, C1 and F-actin only co-localized in the cytoplasm in TRAP<sup>+</sup> mononuclear cells (Figure 7I-7L). Therefore, the destroyed F-actin rings in C1-depleted osteoclasts and the C1 co-localization with F-actin rings, suggest that subunit C1 may be involved in actin sealing ring formation in activated osteoclasts.



## Discussion

Here we demonstrate that *Atp6v1c1* expression is induced by RANKL and M-CSF during osteoclast differentiation, that *Atp6v1c1* silencing can impair osteoclast acidification activity and bone resorption function, that C1 localizes on the ruffled border in vivo in activated osteoclasts, that C1 co-localizes with microtubules in mature osteoclasts and strongly interacts with  $\alpha 3$ , that organized F-actin ring formation is defective in C1-depleted osteoclasts, and that C1 co-localizes with F-actin ring in osteoclasts. Although the subunit C1 expression pattern in mouse tissues [10] and the subunit C bundles of F-actin of varying thickness in vitro [23; 24] have been reported, this is the first report to demonstrate that *Atp6v1c1* is an essential C subunit of the activated osteoclast ruffled border V-ATPase and that it may regulate F-actin sealing ring formation during osteoclast activation.

Our microarray data showed, although *Atp6v1c2* was weakly detected, that *Atp6v1c1* was much more highly expressed (nearly 139-fold) than *Atp6v1c2* in osteoclasts (Figure 1A) and that *Atp6v1c1* expression was 42-fold higher in osteoclasts than in stromal cells (Figure 1B). Sun-Wada et al. reported that the subunit *Atp6v1c1* was ubiquitously expressed in various tissues in mice, but that the other two C subunit isoforms, C2-a and C2-b, were expressed specifically in the lung and kidney, respectively [10;16]. Therefore, we further performed semi-quantitative RT-PCR assays in mouse tissues and cell lines, and verified the higher expression of *Atp6v1c1* in osteoclasts. Although we have detected *Atp6v1c1* expression in brain, kidney, and testis, expression of *Atp6v1c1* was much higher in OCLs and osteoclasts than in MOCIP-5 and BMMs, respectively. In addition, only *Atp6v1c1* (not C2-a or C2-b) was detected in osteoclasts, though *Atp6v1c2* was detected in the brain, lung, kidney, and ES cells (Figure 1C, D). Semi-quantitative assays showed that *Atp6v1c1* expression can be significantly induced by RANKL and M-CSF (Figure 1D). Furthermore, our Western blot results also showed that in the osteoclast primary culture, C1 protein continued to increase through day 4 and stayed at high levels until 7 days after BMMs were treated with RANKL and M-CSF (Figure 1E, F). Here, we report for the first time that C1 (but not C2) is highly expressed in osteoclasts, and that C1 expression can be significantly induced by RANKL and M-CSF.

The high, inducible expression of *Atp6v1c1* in osteoclasts provides evidence that C1 may play a role during osteoclast differentiation, maturation, and activation. To address the question, we knocked down the expression of *Atp6v1c1* using a lentivirus mediated siRNA expression system [27;28;35] and using both  $\alpha 3$ -siRNA and LacZ-siRNA as controls. The results showed that C1 knockdown osteoclasts have normal differentiation and maturation, but impaired acidification activity and bone resorption function (Figure 3A, B, C, D; Figure 4A, B, C). This was similar to  $\alpha 3$ -depleted osteoclasts and is also coincident with the previous report that  $\alpha 3$  knockout mice show normal osteoclast maturation, but decreased extracellular acidification and bone resorption [13]. Our results strongly suggest that *Atp6v1c1* may play a role as an essential component of the osteoclast ruffled border V-ATPase holoenzyme.

During osteoclast activation, V-ATPases polarize to the ruffled border [1], so we performed immunohistochemistry to verify whether C1 also localized in vivo in activated osteoclasts ruffled border. Here, we found that the C1 subunit is much more highly expressed in multinucleated osteoclasts than in surrounding cells and that the main staining was at ruffled border in activated osteoclasts in vivo (Figure 5A, red arrow). As we know, V-ATPase consists of the  $V_1$  and  $V_0$  domains. The  $V_1$  and  $V_0$  domains are connected by a central stalk (composed of subunits D and F of  $V_1$  and subunit d of  $V_0$ ) and by multiple peripheral stalks (composed of subunits C, E, G, and H and the N-terminal domain of subunit a) [2]. Furthermore, the V-ATPase is a tightly coupled enzyme that only exhibits activity when the enzyme is fully assembled with all subunits at the membrane. In yeast, as well as in the tobacco hornworm, subunit C is lost from both sectors during V-ATPase disassociation, suggesting that subunit C

may play a crucial role in the regulation of V-ATPases [36-38]. It has been reported that subunit C interacted with subunit a in yeast [39]. Here, we also found that in osteoclasts, the subunit C1 strongly interacted with a3 by immunoprecipitation (Figure 5B) and that C1, similar to a3 and Atp6v1a, co-localized with microtubules in osteoclasts and their co-localization polarized to the plasma membrane and its vicinity (Figure 5C) [15;40]. C1 has also been shown to interact with the subunit B2 (not B1) in mice [16]. These findings provided further evidence that C1 is an essential component of the osteoclast ruffled border V-ATPase and that its interaction with B2 and a3 may be significant in the connection between V1 and V0 domains.

Osteoclastic bone resorption includes two stages: 1) V-ATPases present in the ruffled border secrete  $H^+$  into the compartment surrounded by the sealing zone; thus, they provide the acidic microenvironment that leads to bone demineralization. This is followed by 2) subsequent degradation of the bone matrix by cathepsin K and matrix metalloproteinases that are secreted into the sealing zone [41]. The sealing zone is associated with a ring of actin filaments [18; 42]. Tehrani et al. also reported that cortactin-based actin assembly is necessary for the sealing ring to function because cortactin-depleted osteoclasts fail to form actin-based sealing rings and fail to resorb bone [35]. Taken together, F-actin assembly to form organized rings is necessary for the osteoclast bone resorption function. In addition, Vitavska et al. recently reported that in the tobacco hornworm, upon V-ATPase dissociation,  $V_1$  complexes do not only detach from the membrane, but also from actin filaments due to the loss of subunit C. Subunit C can bind separately to F-actin, stabilize F-actin, increase the initial rate of actin polymerization in a concentration-dependent manner, and cross-link actin filaments to bundles of varying thickness [23;24]. Their results promote speculation that in addition to Atp6v1c1's function as an essential subunit of the ruffled border V-ATPase, it may be involved in F-actin assembly to form sealing rings in osteoclasts. To test our hypothesis, we depleted *Atp6v1c1* from osteoclasts using RNAi delivered with lentivirus. It is interesting that Atp6v1c1-depleted osteoclasts did not form organized actin rings and that F-actin-containing patches were commonly found in these osteoclasts. In contrast, organized F-actin rings were formed in multinuclear osteoclasts of control groups including Mock, Lenti-LacZ, Lenti-a3 treated cells, and a3<sup>-/-</sup> osteoclasts (Figure 6). Our finding that a3-deleted osteoclasts formed normal F-actin rings is coincident with that in a3<sup>-/-</sup> osteoclasts; it also supports the previous report that Atp6v0a3-deficient osteoclasts form normal F-actin rings [22]. Therefore, it is true that a3 is not involved in F-actin ring formation, which is also consistent with the report that a3 did not co-localize with F-actin rings [15].

Atp6v1c1 deficiency severely impaired F-actin ring formation, so we speculated that C1 co-localizes with F-actin. We performed immunofluorescence to detect C1 and F-actin localization. Besides their co-localization in the cytoplasm (Figure 7A-7L), we found that C1 and F-actin ring localization significantly polarized to the cell periphery in mature multinuclear osteoclasts. Contrastingly, C1 and F-actin co-localized evenly in the cytoplasm (Figure 7I-7L) in TRAP<sup>+</sup> mononuclear cells. The co-localization of C1 and F-actin in osteoclasts suggested that besides being an essential subunit of the V-ATPase, C1 may function as a regulator in normal F-actin ring formation of activated osteoclasts.

Our results showed, for the first time, that Atp6v1c1 plays a role in osteoclast bone resorption as an essential C subunit and may also function as a regulator of F-actin sealing ring formation during osteoclast activation. Furthermore, its expression can be induced by RANKL and M-CSF during osteoclast differentiation, so further studies will be required to identify other molecules that might be involved in the signal pathway by which RANKL and M-CSF activate osteoclasts to form the F-actin sealing ring through C1. Our results showed a high level of C1 expression induced by RANKL (Fig 1E) and an undetectable level of C1 expression in other cells in bone marrow (Fig 1 B, C and E, Fig 5A). So, we suggest that Atp6v1c1 would be a useful target for diseases of bone and cartilage if it is possible to knockdown C1 expression

specifically in bone marrow cells by an approach such as C1 ShRNA Lentivirus infection of bone marrow in vivo (as we did in vitro, Fig 3).

## Acknowledgments

We thank Christie Taylor and Carrie Soltanoff for their manuscript assistance. This work was supported by NIH Grant AR-44741 (Y-P. Li).

## Abbreviations footnote

<b>a3</b>	Atp6v0a3
<b>AO</b>	acridine orange
<b><math>\alpha</math>-MEM</b>	alpha modified Eagle's medium
<b>BMMs</b>	bone marrow-derived monocytes
<b>C1</b>	Atp6v1c1
<b>C2a</b>	Atp6v1c2a
<b>C2b</b>	Atp6v1c2b
<b>d2</b>	Atp6v0d2
<b>DAPI</b>	4',6-diamidino-2-phenylindole
<b>F-actin</b>	filamentous actin
<b>FBS</b>	fetal bovine serum
<b>HEK293T</b>	human embryonic kidney 293T
<b>M-CSF</b>	macrophage-colony stimulating factor
<b>MNCs</b>	multinucleated cells
<b>OCL</b>	osteoclast-like cell
<b>RANKL</b>	receptor activator of NF- $\kappa$ B ligand
<b>TRAP</b>	tartrate-resistant acid phosphatase
<b>V-ATPase</b>	vacuolar ATPase

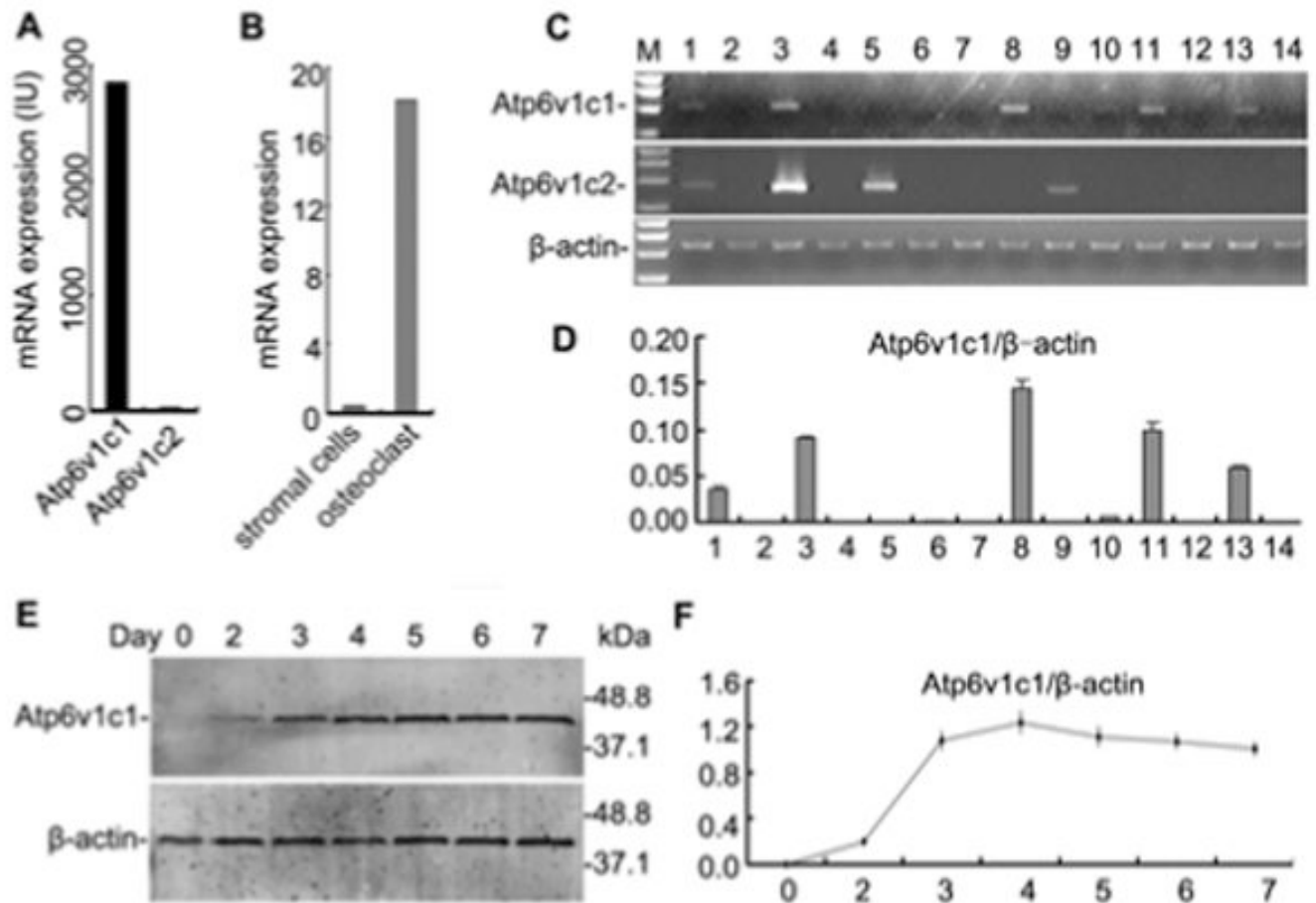
## Reference List

1. Xu J, Cheng T, Feng HT, Pavlos NJ, Zheng MH. Structure and function of V-ATPases in osteoclasts: potential therapeutic targets for the treatment of osteolysis. *Histol Histopathol* 2007;22:443–454. [PubMed: 17290355]
2. Forgac M. Vacuolar ATPases: rotary proton pumps in physiology and pathophysiology. *Nat Rev Mol Cell Biol* 2007;8:917–929. [PubMed: 17912264]
3. Forgac M. Structure and properties of the vacuolar (H<sup>+</sup>)-ATPases. *J Biol Chem* 1999;274:12951–12954. [PubMed: 10224039]
4. Xu T, Vasilyeva E, Forgac M. Subunit interactions in the clathrin-coated vesicle vacuolar (H<sup>+</sup>)-ATPase complex. *J Biol Chem* 1999;274:28909–28915. [PubMed: 10506135]
5. Stevens TH, Forgac M. Structure, function and regulation of the vacuolar (H<sup>+</sup>)-ATPase. *Annu Rev Cell Dev Biol* 1997;13:779–808. [PubMed: 9442887]

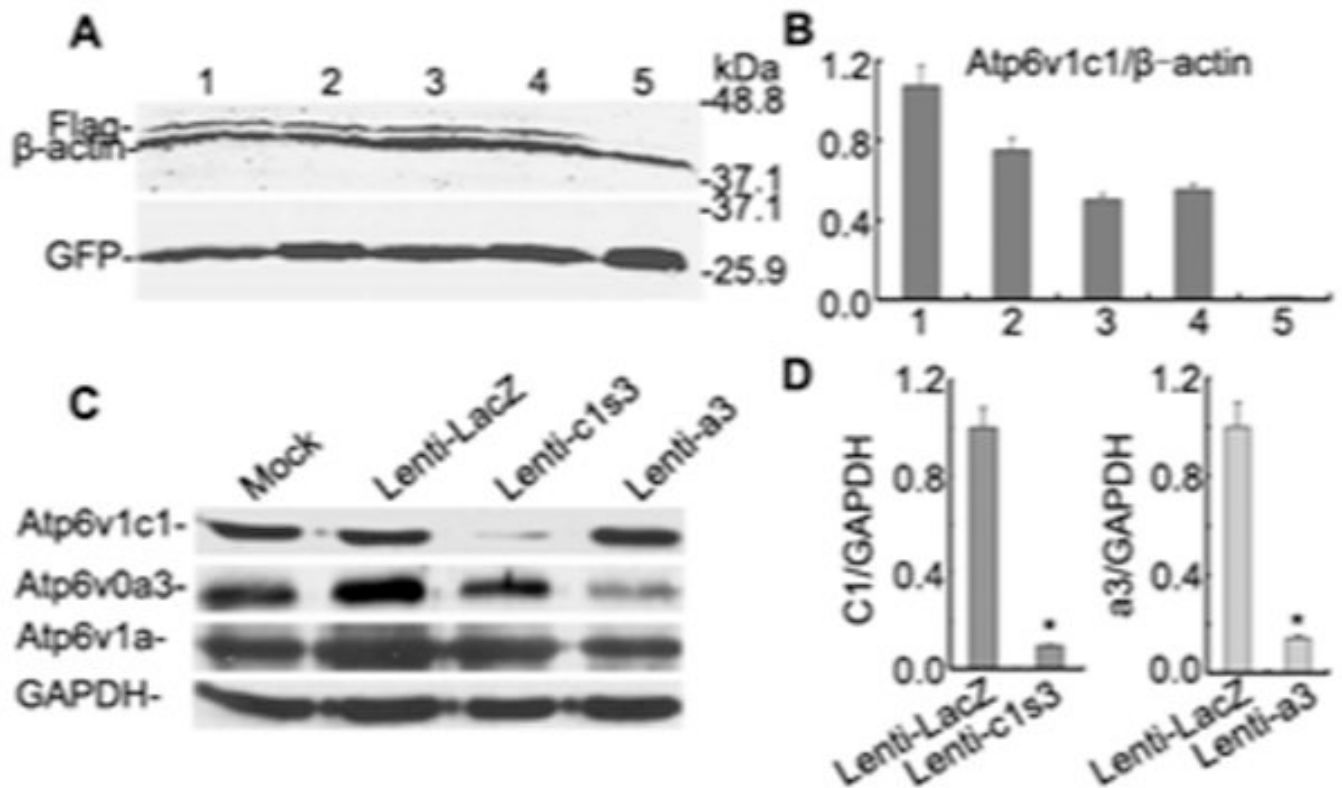
6. Nishi T, Kawasaki-Nishi S, Forgac M. Expression and function of the mouse V-ATPase d subunit isoforms. *J Biol Chem* 2003;278:46396–46402. [PubMed: 12963731]
7. Paunescu TG, Da SN, Marshansky V, McKee M, Breton S, Brown D. Expression of the 56-kDa B2 subunit isoform of the vacuolar H(+)-ATPase in proton-secreting cells of the kidney and epididymis. *Am J Physiol Cell Physiol* 2004;287:C149–C162. [PubMed: 15013950]
8. Pietrement C, Sun-Wada GH, Silva ND, McKee M, Marshansky V, Brown D, Futai M, Breton S. Distinct expression patterns of different subunit isoforms of the V-ATPase in the rat epididymis. *Biol Reprod* 2006;74:185–194. [PubMed: 16192400]
9. Smith AN, Borthwick KJ, Karet FE. Molecular cloning and characterization of novel tissue-specific isoforms of the human vacuolar H(+)-ATPase C, G and d subunits, and their evaluation in autosomal recessive distal renal tubular acidosis. *Gene* 2002;297:169–177. [PubMed: 12384298]
10. Sun-Wada GH, Yoshimizu T, Imai-Senga Y, Wada Y, Futai M. Diversity of mouse proton-translocating ATPase: presence of multiple isoforms of the C, d and G subunits. *Gene* 2003;302:147–153. [PubMed: 12527205]
11. Murata Y, Sun-Wada GH, Yoshimizu T, Yamamoto A, Wada Y, Futai M. Differential localization of the vacuolar H<sup>+</sup> pump with G subunit isoforms (G1 and G2) in mouse neurons. *J Biol Chem* 2002;277:36296–36303. [PubMed: 12133826]
12. Lee BS, Holliday LS, Ojikutu B, Krits I, Gluck SL. Osteoclasts express the B2 isoform of vacuolar H(+)-ATPase intracellularly and on their plasma membranes. *Am J Physiol* 1996;270:C382–C388. [PubMed: 8772466]
13. Li YP, Chen W, Liang Y, Li E, Stashenko P. Atp6i-deficient mice exhibit severe osteopetrosis due to loss of osteoclast-mediated extracellular acidification. *Nat Genet* 1999;23:447–451. [PubMed: 10581033]
14. Kornak U, Kasper D, Bosl MR, Kaiser E, Schweizer M, Schulz A, Friedrich W, Delling G, Jentsch TJ. Loss of the ClC-7 chloride channel leads to osteopetrosis in mice and man. *Cell* 2001;104:205–215. [PubMed: 11207362]
15. Toyomura T, Murata Y, Yamamoto A, Oka T, Sun-Wada GH, Wada Y, Futai M. From lysosomes to the plasma membrane: localization of vacuolar-type H<sup>+</sup> -ATPase with the α3 isoform during osteoclast differentiation. *J Biol Chem* 2003;278:22023–22030. [PubMed: 12672822]
16. Sun-Wada GH, Murata Y, Namba M, Yamamoto A, Wada Y, Futai M. Mouse proton pump ATPase C subunit isoforms (C2-a and C2-b) specifically expressed in kidney and lung. *J Biol Chem* 2003;278:44843–44851. [PubMed: 12947086]
17. Faccio R, Grano M, Colucci S, Villa A, Giannelli G, Quaranta V, Zallone A. Localization and possible role of two different α v β 3 integrin conformations in resting and resorbing osteoclasts. *J Cell Sci* 2002;115:2919–2929. [PubMed: 12082152]
18. Saltel F, Destaing O, Bard F, Eichert D, Jurdic P. Apatite-mediated actin dynamics in resorbing osteoclasts. *Mol Biol Cell* 2004;15:5231–5241. [PubMed: 15371537]
19. Pfaff M, Jurdic P. Podosomes in osteoclast-like cells: structural analysis and cooperative roles of paxillin, proline-rich tyrosine kinase 2 (Pyk2) and integrin αVβ3. *J Cell Sci* 2001;114:2775–2786. [PubMed: 11683411]
20. Lee SH, Rho J, Jeong D, Sul JY, Kim T, Kim N, Kang JS, Miyamoto T, Suda T, Lee SK, Pignolo RJ, Koczon-Jaremko B, Lorenzo J, Choi Y. v-ATPase V0 subunit d2-deficient mice exhibit impaired osteoclast fusion and increased bone formation. *Nat Med* 2006;12:1403–1409. [PubMed: 17128270]
21. Hu Y, Nyman J, Muhonen P, Vaananen HK, Laitala-Leinonen T. Inhibition of the osteoclast V-ATPase by small interfering RNAs. *FEBS Lett* 2005;579:4937–4942. [PubMed: 16115623]
22. Taranta A, Migliaccio S, Recchia I, Caniglia M, Luciani M, De RG, onisi-Vici C, Pinto RM, Francalanci P, Boldrini R, Lanino E, Dini G, Morreale G, Ralston SH, Villa A, Vezzoni P, Del PD, Cassiani F, Palumbo G, Teti A. Genotype-phenotype relationship in human ATP6i-dependent autosomal recessive osteopetrosis. *Am J Pathol* 2003;162:57–68. [PubMed: 12507890]
23. Vitavska O, Merzendorfer H, Wiczorek H. The V-ATPase subunit C binds to polymeric F-actin as well as to monomeric G-actin and induces cross-linking of actin filaments. *J Biol Chem* 2005;280:1070–1076. [PubMed: 15525650]
24. Vitavska O, Wiczorek H, Merzendorfer H. A novel role for subunit C in mediating binding of the H<sup>+</sup>-V-ATPase to the actin cytoskeleton. *J Biol Chem* 2003;278:18499–18505. [PubMed: 12606563]

25. Yang S, Li YP. RGS12 is essential for RANKL-evoked signaling for terminal differentiation of osteoclasts in vitro. *J Bone Miner Res* 2007;22:45–54. [PubMed: 17042716]
26. Chen W, Li YP. Generation of mouse osteoclastogenic cell lines immortalized with SV40 large T antigen. *J Bone Miner Res* 1998;13:1112–1123. [PubMed: 9661075]
27. Kissler S, Stern P, Takahashi K, Hunter K, Peterson LB, Wicker LS. In vivo RNA interference demonstrates a role for Nramp1 in modifying susceptibility to type 1 diabetes. *Nat Genet* 2006;38:479–483. [PubMed: 16550170]
28. Stewart SA, Dykxhoorn DM, Palliser D, Mizuno H, Yu EY, An DS, Sabatini DM, Chen IS, Hahn WC, Sharp PA, Weinberg RA, Novina CD. Lentivirus-delivered stable gene silencing by RNAi in primary cells. *RNA* 2003;9:493–501. [PubMed: 12649500]
29. Murrills RJ, Dempster DW. The effects of stimulators of intracellular cyclic AMP on rat and chick osteoclasts in vitro: validation of a simplified light microscope assay of bone resorption. *Bone* 1990;11:333–344. [PubMed: 1701319]
30. Yang S, Chen W, Stashenko P, Li YP. Specificity of RGS10A as a key component in the RANKL signaling mechanism for osteoclast differentiation. *J Cell Sci* 2007;120:3362–3371. [PubMed: 17881498]
31. Yang S, Li YP. RGS10-null mutation impairs osteoclast differentiation resulting from the loss of  $[Ca^{2+}]_i$  oscillation regulation. *Genes Dev* 2007;21:1803–1816. [PubMed: 17626792]
32. Baron R, Neff L, Louvard D, Courtot PJ. Cell-mediated extracellular acidification and bone resorption: evidence for a low pH in resorbing lacunae and localization of a 100-kD lysosomal membrane protein at the osteoclast ruffled border. *J Cell Biol* 1985;101:2210–2222. [PubMed: 3905822]
33. Toyomura T, Oka T, Yamaguchi C, Wada Y, Futai M. Three subunit a isoforms of mouse vacuolar H(+)-ATPase. Preferential expression of the a3 isoform during osteoclast differentiation. *J Biol Chem* 2000;275:8760–8765. [PubMed: 10722719]
34. Blair HC, Teitelbaum SL, Ghiselli R, Gluck S. Osteoclastic bone resorption by a polarized vacuolar proton pump. *Science* 1989;245:855–857. [PubMed: 2528207]
35. Tehrani S, Faccio R, Chandrasekar I, Ross FP, Cooper JA. Cortactin has an essential and specific role in osteoclast actin assembly. *Mol Biol Cell* 2006;17:2882–2895. [PubMed: 16611741]
36. Parra KJ, Keenan KL, Kane PM. The H subunit (Vma13p) of the yeast V-ATPase inhibits the ATPase activity of cytosolic V1 complexes. *J Biol Chem* 2000;275:21761–21767. [PubMed: 10781598]
37. Kane PM. Disassembly and reassembly of the yeast vacuolar H(+)-ATPase in vivo. *J Biol Chem* 1995;270:17025–17032. [PubMed: 7622524]
38. Sumner JP, Dow JA, Earley FG, Klein U, Jager D, Wiczorek H. Regulation of plasma membrane V-ATPase activity by dissociation of peripheral subunits. *J Biol Chem* 1995;270:5649–5653. [PubMed: 7890686]
39. Inoue T, Forgac M. Cysteine-mediated cross-linking indicates that subunit C of the V-ATPase is in close proximity to subunits E and G of the V1 domain and subunit a of the V0 domain. *J Biol Chem* 2005;280:27896–27903. [PubMed: 15951435]
40. bu-Amer Y, Ross FP, Schlesinger P, Tondravi MM, Teitelbaum SL. Substrate recognition by osteoclast precursors induces C-src/microtubule association. *J Cell Biol* 1997;137:247–258. [PubMed: 9105052]
41. Henriksen K, Sorensen MG, Nielsen RH, Gram J, Schaller S, Dziegiel MH, Everts V, Bollerslev J, Karsdal MA. Degradation of the organic phase of bone by osteoclasts: a secondary role for lysosomal acidification. *J Bone Miner Res* 2006;21:58–66. [PubMed: 16355274]
42. Kanehisa J, Yamanaka T, Doi S, Turksen K, Heersche JN, Aubin JE, Takeuchi H. A band of F-actin containing podosomes is involved in bone resorption by osteoclasts. *Bone* 1990;11:287–293. [PubMed: 2242294]



**Figure 1.**

Expression of *Atp6v1c1* in osteoclasts. (A) Microarray data of expression levels of *Atp6v1c1* and *Atp6v1c2* in human osteoclasts. (B) Microarray data of the expression level of *Atp6v1c1* in stromal cells and human osteoclasts. (C) Semi-quantitative RT-PCR assays in eight mouse tissues (M: molecular marker; lanes 1-8: brain, heart, kidney, liver, lung, ovary, spleen, and testis) and six related cells (lanes 9-14: ES, MOCP-5, OCL, BMMs, OC, and OB) were performed with gene-specific primers for *Atp6v1c1*, *Atp6v1c2* (the common primers for *c2a* and *c2b*), and  $\beta$ -actin. (D) Quantification of *Atp6v1c1* expression level (normalized to the  $\beta$ -actin level) ( $n=3$ ). (E) Time course of *Atp6v1c1* protein in RANKL- (10 ng/ml) and M-CSF- (10 ng/ml) stimulated BMMs by Western blotting. (F) Quantification of *Atp6v1c1* protein expression level during osteoclast differentiation and maturation (normalized to the  $\beta$ -actin level) ( $n=3$ ).

**Figure 2.**

Validation of the depletion effect of siRNA targeting *Atp6v1c1*. (A) Effective siRNA target sequence selection on over-expressed Flag-C1 in HEK-293T by Western blotting. We used anti- $\beta$ -actin as a protein loading control and anti-GFP as a transfection efficiency control. Lane 1, pSUPER+Flag-C1; Lane 2, pSUPER-LacZ+Flag-C1; Lane 3, pSUPER-c1s1+Flag-C1; Lane 4, pSUPER-c1s2+Flag-C1; Lane 5, pSUPER-c1s3+Flag-C1. (B) Quantification of expression of Flag-C1 (normalized to the  $\beta$ -actin level) in lanes as above (n=3). (C) Verified c1s3 knockdown effect by lentivirus-mediated transduction of primary culture osteoclasts on day 2, induced by RANKL and M-CSF. (D) Quantification of expressions of *Atp6v1c1* and *Atp6v0a3* (normalized to the  $\beta$ -actin level) (n=3). \*  $P < 0.05$  compared with that of Lenti-LacZ treated cells.

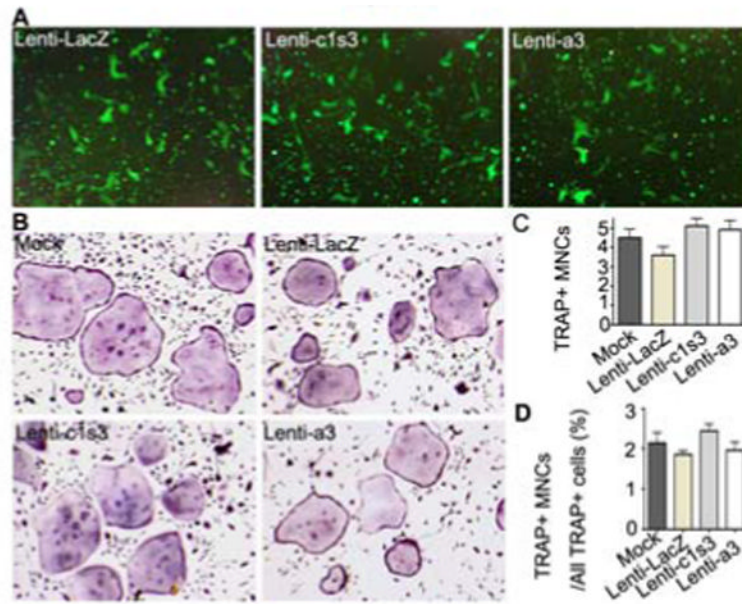


**Figure 3.** Normal differentiation and maturation of osteoclasts depleted of *Atp6v1c1*. (A) All cells expressed GFP, showing that cells were infected by lentivirus and also expressed siRNA. (B) TRAP staining of osteoclasts. (C) Quantification of TRAP<sup>+</sup> OCLs ( $\geq 3$  nuclei) per random view. (D) The percentage of TRAP<sup>+</sup> OCLs ( $\geq 3$  nuclei) in all TRAP<sup>+</sup> cells per random view. All data are expressed as mean  $\pm$  s.d. (n=10).

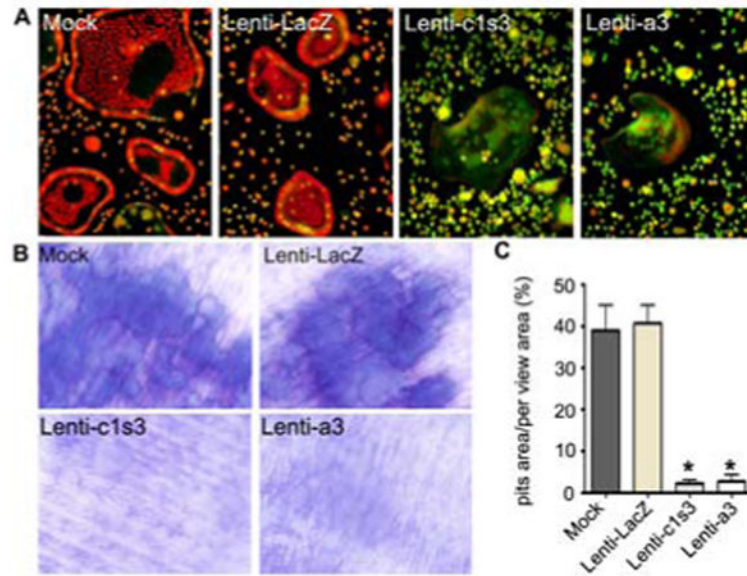


**Figure 4.**

Depletion of *Atp6v1c1* blocked the acidification activity of osteoclasts and decreased bone resorption of osteoclasts. (A) Acridine orange staining of osteoclasts including cells without fusion (< 3 nuclei). (B) Patterns of resorption pits on dentin slices. (C) Quantification of resorption area per view area. Results are mean  $\pm$  s.e.m. (n=3). \*  $P < 0.05$  compared with that of Lenti-LacZ treated cells.

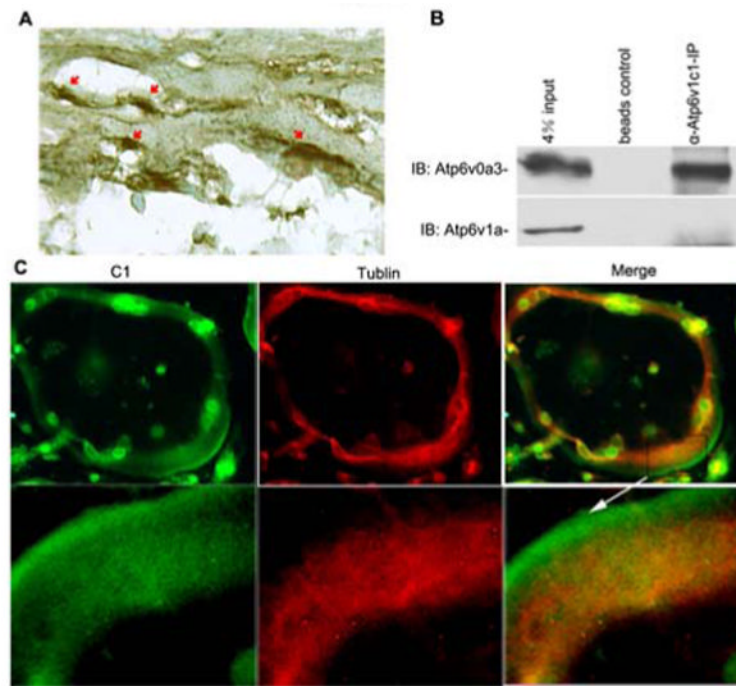


**Figure 5.**

Atp6v1c1 interacted with a3 in osteoclasts and it localized towards the bone surface in vivo in activated osteoclasts. (A) Anti-Atp6v1c1 immunostaining of 10-day-old mouse tibiae. Atp6v1c1 was much more highly expressed in multinucleated osteoclasts and the main staining is at ruffled border (red arrow). (B) Co-immunoprecipitation of Atp6v1c1 with a3 or Atp6v1a. Interaction was observed between C1 and a3 subunits but no interaction was observed between C1 and A subunits. (C) Atp6v1c1 co-localized with microtubules and polarized to the plasma membrane and its vicinity in mature osteoclasts and C1 staining formed a belt at the cell periphery. The cells shown were the representative of the data (n=3).



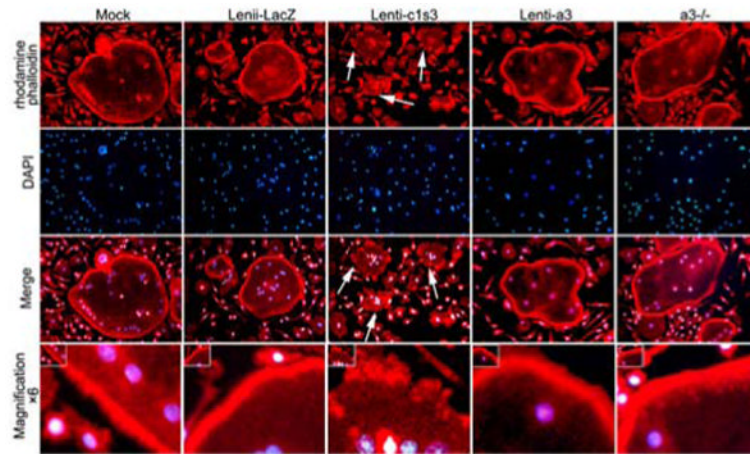


**Figure 6.**

Depletion of *Atp6v1c1* blocked F-actin ring formation. Lentivirus treated cells and *a3*<sup>-/-</sup> osteoclasts were stained with rhodamine phalloidin for F-actin rings. Nuclei were visualized with DAPI. F-actin-containing patches are commonly found in C1 knockdown osteoclasts (white arrow), which unlike mock, Lenti-*a3*, or Lenti-LacZ, infected osteoclasts or *a3*<sup>-/-</sup> osteoclasts, fail to develop an organized actin belt at the cell periphery. The cells shown were the representative of the data (n=4).

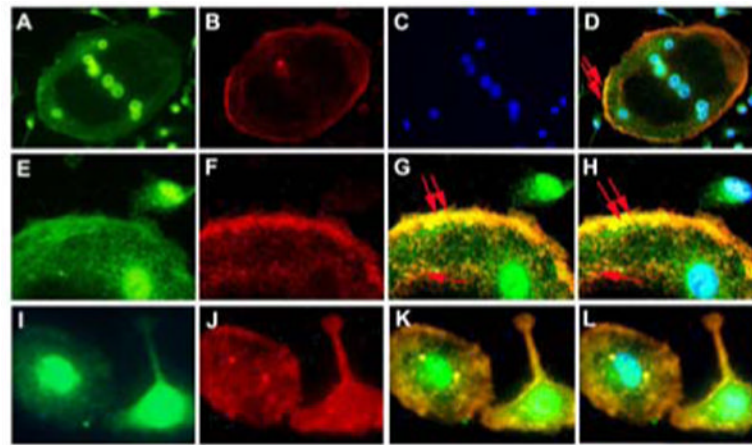


**Figure 7.**

Atp6v1c1 co-localization with F-actin in osteoclasts. (A, E, I) Staining with  $\alpha$ -Atp6v1c1. (A) Mature osteoclast. (E) High magnification of A. (I) Mononuclear TRAP<sup>+</sup> cells. (B, F, G) F-actin rhodamine phalloidin staining. (B) Mature osteoclast. (F) High magnification of B. (J) Mononuclear TRAP<sup>+</sup> cells. (C) Nuclei were visualized with DAPI. (D) The merge of A, B, and C. (G) The merge of E and F. (H) The merge of G and nuclei. (K) The merge of I and J. (L) The merge of K and nuclei. Besides the co-localization in the cytoplasm (single red arrow; D, G, H), Atp6v1c1 localization moved to the cell periphery along with the F-actin ring (double red arrows) in mature multinucleated osteoclasts. In TRAP<sup>+</sup> mononuclear cells, C1 and F-actin co-localized in the cytoplasm evenly (K, L). The cells shown were the representative of the data (n=3).